ACI STRUCTURAL JOURNAL TECHNICAL PAPER

Title No. 115-S68

Impact of Geometry and Detailing on Drift Capacity of Slender Walls

by Christopher L. Segura Jr. and John W. Wallace

*Recent earthquakes and laboratory tests have demonstrated that thin, slender walls may not possess the deformation levels allowed in U.S. codes and standards. A study of the lateral drift capacity of well-detailed walls was conducted, indicating equivalent performance is not expected for all walls that satisfy ACI 318-14 provisions. A lateral drift capacity prediction equation was developed in a displacement-based design format and was shown to agree with experimentally measured drift capacities for a small database of slender wall laboratory tests. It was demonstrated that, in addition to provided boundary transverse reinforcement, drift capacity of slender walls is most impacted by compression depth (*c*), wall thickness (*b*), and wall length (l_w). Based on experimental data, drift capacities greater than 2% may be expected for code-compliant walls designed such that* $c/b < 2.5$*, while drifts lower than 1% are expected when* $c/b > 5.0$.

Keywords: boundary element; compression strain; confinement; detailing; drift capacity; reinforced concrete; shear wall, structural wall; wall thickness.

INTRODUCTION

ACI 318-14 design provisions for slender walls are based on research that has demonstrated that large lateral drift ratios can be achieved when compression zones in yielding regions are adequately detailed to remain stable (for example, Oesterle et al. [1976], Paulay and Goodsir [1985], Thomsen and Wallace [1995], and Brueggen et al. [2017]). However, recent studies (Wallace 2012) and laboratory tests (Nagae et al. 2012; Lowes et al. 2012; Segura and Wallace 2018) have revealed that code-compliant walls may experience brittle compression failure prior to reaching the lateral drift limits or plastic rotations allowed by U.S. design codes and standards (that is, ASCE 7, ASCE 41). Segura and Wallace (2018) studied the relationship between wall thickness and lateral drift capacity, finding that thin walls (for example, less than approximately 12 in. [305 mm] thick) may possess smaller lateral drift capacities than thicker walls that are otherwise similar. Furthermore, it has been found that thin, rectangular sections confined by an outer hoop and crossties, which is a detail allowed by ACI 318-14 at wall boundaries, may be substantially less stable in compression than those using overlapping hoops, without crossties, for confinement (Welt 2015; Segura and Wallace 2018). Drift limitations for thin walls are not currently addressed in ACI 318; instead, it is assumed that all walls satisfying ACI 318-14 Special Structural Wall provisions possess adequate ductility to meet the drift demands.

Experimental data from the tests conducted by Segura and Wallace (2018) are used to identify performance limitations (axial compression and tension strain limits) for code-compliant walls in which the lateral drift capacity is limited by flexure-compression (concrete crushing and longitudinal reinforcement buckling) or flexure-tension (fracture of longitudinal reinforcement). Extreme fiber strain limits identified in the tests are used to formulate a relationship to predict the lateral drift capacity of code-compliant walls as a function of wall thickness (b), wall length (l_w), and compression depth (c). In addition, experimentally measured drift capacities are presented for a small database of well-detailed walls, and it is demonstrated that the drift prediction formulation is in good agreement with the experimental data for the walls in the database.

RESEARCH SIGNIFICANCE

Despite recent changes to ACI 318-14, the role of wall thickness and confinement detailing on slender wall performance have not been fully addressed. Because of the widespread use of slender walls in areas impacted by strong earthquakes, it is critical to understand the design conditions (for example, wall thickness, compression depth) for which walls designed to current ACI provisions do not provide sufficient drift capacity. It is equally important to identify the conditions for which current code requirements provide adequate drift capacity, so that all walls are not required to be detailed for the worst-case scenario.

LATERAL DEFORMATIONS IN SLENDER WALLS

The lateral displacement at the top of a cantilever wall (δ_u) is composed of the flexural and shear responses (that is, $\delta_u = \delta_f + \delta_s$). Slender walls are designed to yield in flexure prior to reaching the shear strength of the wall; thus, the inelastic response is dominated by flexural behavior. Figure 1 presents the plastic hinge model formulation used to express the lateral flexural displacement (δ_f) at the top of a cantilever wall in terms of elastic drift ($\delta_{f,y}$) and inelastic drift ($\delta_{f,p}$). For a cantilever wall that is effectively continuous from the base of the structure to the top of the wall, flexural yielding occurs at the bottom of the wall where the overturning moment is largest. Inelastic drift is assumed to occur as plastic rotation (θ_p) centered about the centroid of the plastic curvature profile ($\bar{x}$ in Fig. 1). For a known plastic curvature profile, denoted $\phi_p(x)$ in Fig. 1(a), θ_p can be

ACI Structural Journal, V. 115, No. 3, May 2018.
MS No. S-2017-221, doi: 10.14359/51702046, was received June 20, 2017, and reviewed under Institute publication policies.

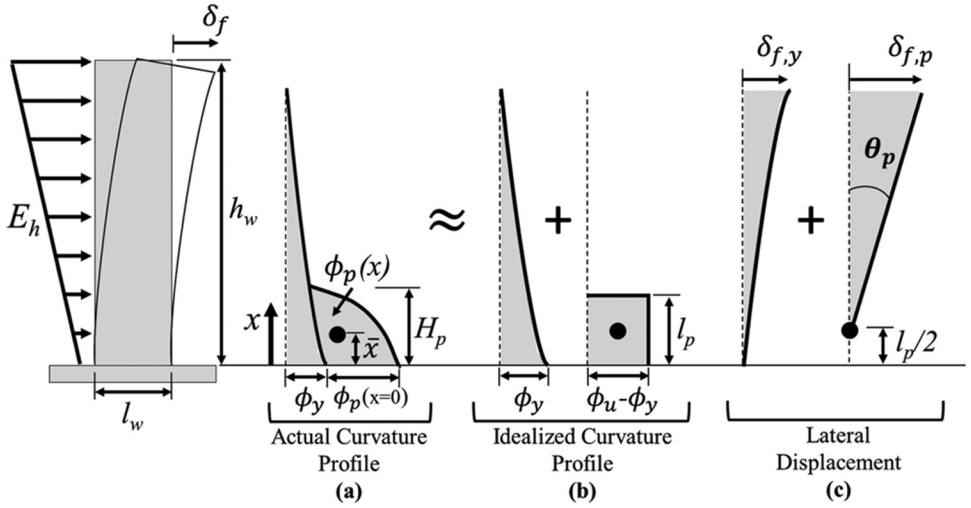

Fig. 1—Cantilever wall curvature profile and lateral flexural displacement.

determined by integrating $\phi_p(x)$ over the height of the plastic curvature profile (denoted H_p in Fig. 1): $\theta_p = \int_0^{H_p} \phi_p(x)dx$. As illustrated in Fig. 1(b), it is common to idealize plastic curvature as constant over an assumed plastic hinge length (l_p), in which case δ_f may be expressed by Eq. (1)

$$\delta_f = \delta_{f,y} + \delta_{f,p} = \delta_{f,y} + \theta_p(h_w - \bar{x}) = \delta_{f,y} + (\phi_u - \phi_y)l_p(h_w - l_p/2) \quad (1)$$

where ϕ_y is the curvature at yielding of longitudinal reinforcement; and ϕ_u is the ultimate curvature associated with δ_f and l_p. Assuming plane sections remain plane, ϕ_u in Eq. (1) can be defined as the extreme fiber compression strain (ε_c) divided by the compression depth (c), leading to the definition of θ_p and $\delta_{f,p}$ in Eq. (2a) and (2b), respectively. At large ductility demands ($\phi_u \approx \phi_u - \phi_y$), Eq. (2b) can be simplified (Eqn. (2c)) by recognizing that θ_p is nearly equal to $\delta_{f,p}/h_w$ (that is, $h_w \approx h_w - l_p/2$); hence, plastic drift ($\delta_{f,p}/h_w$) can be directly related to extreme fiber compression strain for an assumed plastic hinge length and a given compression depth, typically assumed to be relatively constant for $\varepsilon_c \geq 0.003$

$$\theta_p = \left(\frac{\varepsilon_c}{c} - \phi_y\right) l_p \quad (2a)$$

$$\frac{\delta_{f,p}}{h_w} = \frac{1}{h_w}\left(\frac{\varepsilon_c}{c} - \phi_y\right) l_p (h_w - l_p/2) \quad (2b)$$

$$\frac{\delta_{f,p}}{h_w} \approx \theta_p \approx \frac{\varepsilon_c}{c} l_p \quad (2c)$$

For ACI 318-99 through 318-14, detailing of slender walls is based on Eq. (2c) (Wallace and Orakcal 2002). Special Boundary Element (SBE) detailing (that is, boundary transverse reinforcement) is required if Eq. (2c) indicates $\varepsilon_c \geq 0.003$, commonly associated with crushing of unconfined concrete, for the design roof displacement (δ_u). In ACI 318, a plastic hinge length of one-half the length of the wall ($l_p = l_w/2$) is assumed, and inelastic flexural displacement is assumed to be equal to the design displacement (that is, $\delta_u \approx \delta_{f,p}$). This is considered conservative because δ_u, which is determined by a structural analysis of the building, also includes elastic flexural and shear deformations. Other than the requirement for SBEs, ACI 318 does not place a limit on compression strain or lateral drift for slender walls.

DEFORMATION AND STRAIN CAPACITY OF SLENDER WALLS

Laboratory tests on walls with SBE detailing (Nagae et al. 2012; Lowes et al. 2012; Segura and Wallace 2018) indicate a drift or strain limit may be necessary to avoid brittle compression failure in well-detailed walls. The objectives of the wall tests conducted by Segura and Wallace (2018) were to identify the causes of poor performance of walls in recent earthquakes and laboratory tests, and to quantify critical design limitations (for example, compression and tension strain limits, minimum wall thickness) that could be incorporated into future building code releases. Data from these tests are used in the following sections; therefore, pertinent information is presented for the experimental program. The reader is referred to the research report (Segura 2017) for a detailed discussion of the test specimens, experimental setup, instrumentation, and loading protocol. Figure 2 shows cross-sectional geometry and reinforcement details of the seven, approximately one-half scale, wall panel specimens which represented approximately the bottom 1.5 stories of an eight-story cantilever wall. The specimens ranged between 6 and 9 in. (152 and 229 mm) in thickness, and were all 90 in. (2286 mm) in length and 84 in. (2134 mm) in height. SBE detailing was provided at the boundaries of all seven walls, except at the thick, flange boundary of Specimen WP4. At the boundaries of Specimens WP1 to WP4, and at the east boundaries of WP6 and WP7, confinement consisted of a single outer hoop with crossties. For Specimen WP5, and at the west boundaries of specimens WP6 and WP7, continuous transverse reinforcement, which is similar to overlapping hoops, was used.

The test setup and instrumentation layout are shown in Fig. 3. Loading was applied using two vertical actua-

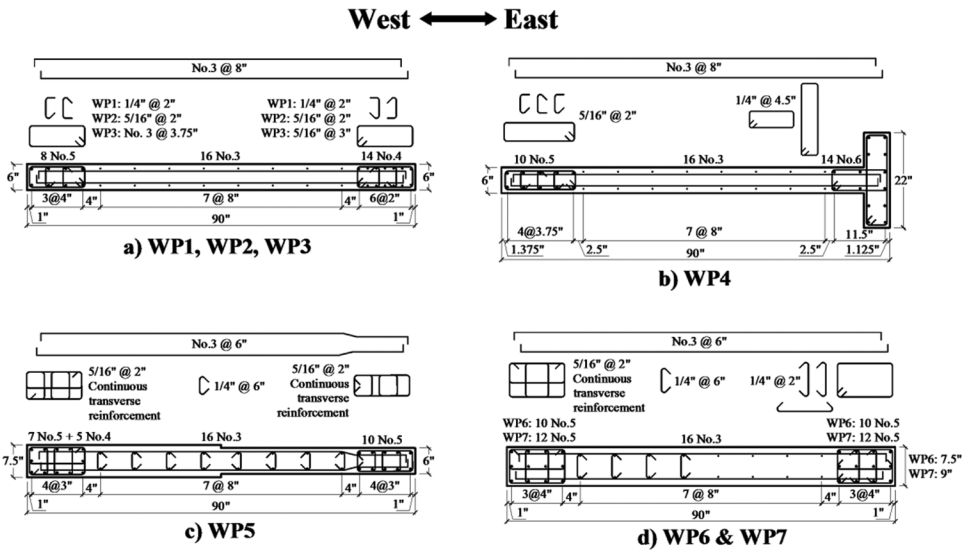

Fig. 2—Reinforcement layout: (a) Specimens WP1, WP2, and WP3; (b) Specimen WP4; (c) Specimen WP5; and (d) Specimens WP6 and WP7. (Note: 1 in. = 25.4 mm.)

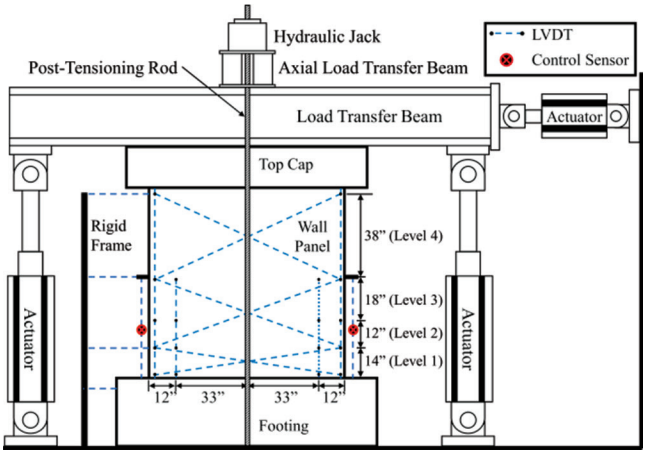

Fig. 3—Test setup and instrumentation layout. (Note: 1 in. = 25.4 mm.)

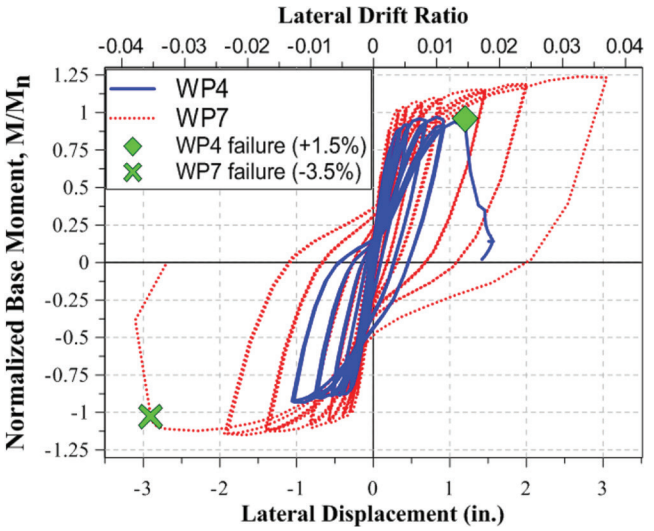

*Fig. 4—Normalized base moment versus lateral drift at top of specimen for Specimens WP4 (*b *= 6 in. [152 mm]) and WP7 (*b *= 9 in. [229 mm]). (Note: 1 in. = 25.4 mm.)*

tors, one horizontal actuator, and two hydraulic jacks. The vertical actuators applied a moment couple to the top of the wall panels, and the horizontal actuator applied shear and additional overturning moment. The applied moment and shear force were representative of the demands given by ASCE 7-10 Equivalent Lateral Force Procedure (ASCE/SEI 2010) at the bottom of an eight-story wall with constant story height and story mass up the height of the wall. Most of the axial load was applied by the two hydraulic jacks, and the remainder was applied using the two vertical actuators. In addition to the instrumentation shown in Fig. 3, a digital image correlation (DIC) system was used to measure strains on the surface of specimens. The DIC system consists of a software package (Barthès 2015), digital single-lens reflex cameras, and lighting equipment. The front surface of each specimen was prepared with a random pattern of black paint speckles atop a white painted surface, and high-resolution images of the specimens were taken throughout the tests. The resulting pixelated images possess a unique grayscale pattern. The DIC software computes surface strains by comparing the deformation of small subsets of this grayscale pattern to an undeformed reference image.

Experimentally measured base moment versus top lateral displacement responses are presented in Fig. 4 for one of the thinnest walls tested (WP4; b = 6 in. [152 mm]) and the thickest wall tested (WP7; b = 9 in. [229 mm]). Of the seven specimens, WP4 and WP7 demonstrated the smallest drift capacity and largest drift capacity, respectively. The displacements reported in Fig. 4 were measured by sensors 82 in. (2083 mm) above the specimen footings (Fig. 3), which is approximately the middle of the second story in the full-height prototype wall. Thus, lateral drift ratios in Fig. 4 are essentially first-story interstory drifts. Except for WP5, brittle compression failures were observed for all the 6 in. (152 mm) thick walls prior to reaching lateral interstory drift ratios expected for Design Earthquake (DE) and Maximum Considered Earthquake (MCE) demands, which could approach 2% and 3%, respectively. Compression

failures were also observed for Specimens WP6 and WP7, which were 25% and 50% thicker than WP1 through WP4, although interstory drift ratios of at least 3% were measured prior to failure. It is noted that lateral drift demands are typically determined for the DE spectra, which are defined in ASCE 7 as two-thirds of the MCE spectra. Thus, to meet the performance objective of ASCE 7 of a low probability of collapse for MCE demands, it may be reasonable to require code-compliant walls to demonstrate interstory drift capacities that are at least 1.5 times the interstory drift ratio allowed by code. This means that code-compliant walls in buildings classified as Seismic Risk Category I or II may be expected to possess interstory drift capacities on the order of 3%, which was not the case for the thinnest specimens (WP1 to WP5). To achieve drift ratios greater than 2% and 3%, it may be necessary to impose a minimum wall thickness requirement. Alternatively, a variable drift limit, which accounts for lower drift capacities of thin walls, could be implemented. To this end, a compression strain limit (ε_{cu}) of 0.008 has been enforced in the Chilean reinforced concrete standard DS No. 60 (MINVU 2011), based on research conducted following the 2010 Maule earthquake (Massone 2013). The compression strain limit in the Chilean code is intended for walls in stiff buildings with detailing similar to that required by ACI 318-14 Section 18.10.6.5, which is less stringent than SBE detailing (ACI 318-14 Section 18.10.6.4). The strain limit has been implemented in a displacement-based design (DBD) format, similar to Eq. (2a) to (2c), assuming $\varepsilon_{cu} = 0.008$ and $l_p = l_w/2$. DS No. 60 estimates roof drift as plastic rotation about the base of the wall (that is, $\delta_u/h_w \approx \theta_p$), and elastic curvature may either be included (DS No. 60 Eq. 21-7b), in keeping with Eq. (2a), or neglected (DS No. 60 Eq. 21-7a). For the case in which elastic curvature is neglected (Eq. (2c)), the drift limit (δ_{max}/h_w) can be determined in accordance with Eq. (3)

$$\frac{\delta_{max}}{h_w} = \frac{\varepsilon_{cu} l_p}{c} = \frac{\varepsilon_{cu}}{2(c/l_w)} \quad (3)$$

Figure 5 presents axial strain profiles for Specimens WP2, WP4, and WP7 measured prior to strength loss, defined herein as a 20% reduction in lateral strength from peak capacity. The reported strains were measured over a gauge length of approximately $l_w/2$ (44 in. [1118 mm]), which is consistent with the assumed plastic hinge length in Eq. (3). The maximum measured extreme fiber compression strain for WP2 (ε_{cu} = 0.0092), WP4 (ε_{cu} = 0.0079), and WP7 (ε_{cu} = 0.012) each exceeded or closely matched the 0.008 Chilean strain limit. With the exception of Specimens WP3 (ε_{cu} = 0.0063) and WP7 (ε_{cu} = 0.012), maximum compression strain measurements ranged between 0.008 and 0.009 (Segura 2017). The results suggest that the 0.008 compression strain limit enforced in the Chilean code may be suitable for thin, code-compliant walls, which is discussed in further detail later. It is noted that ACI 318-14 limits the spacing of boundary transverse reinforcement to one-third of the compression zone thickness ($s \le b/3$). The 3 in. (76 mm) and 3.75 in. (95 mm) spacings at the east and west boundaries of

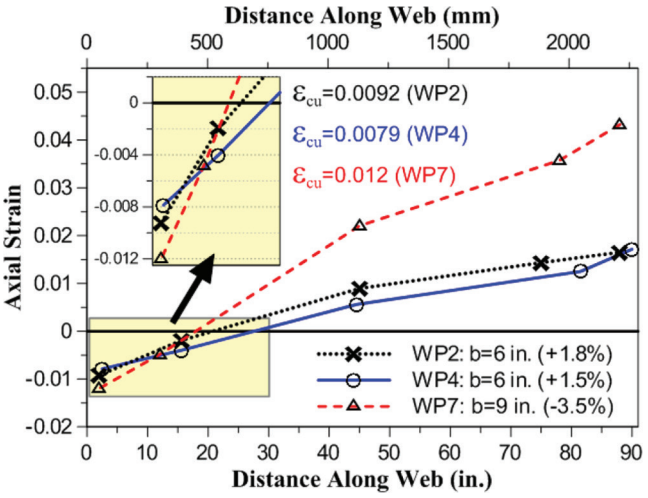

*Fig. 5—Axial strain profiles prior to strength loss for Specimens WP2 (*b *= 6 in. [152 mm]), WP4 (*b *= 6 in.; [152 mm]), and WP7 (*b *= 9 in. [229 mm]). Strains measured over gauge length equal to approximately* $l_w/2$ *(44 in. [1118 mm]).*

Specimen WP3 (b = 6 in. [152 mm]), for which the smallest ε_{cu} value was measured, both exceeded the 2 in. (51 mm) limit imposed by this requirement.

To evaluate the validity of a DBD drift limit (for example, Eq. (3)) using the extreme fiber compression strain limits identified in Fig. 5, a small database of tests conducted on thin, well-detailed rectangular and T-shape walls was assembled. Test specimens were included in the database because they satisfied the following criteria: 1) the shear span-depth ratio (M/Vl_w) was at least 2.0 (slender wall); 2) the wall was designed for moderate to high compression depth (that is, $c/l_w > 0.10$); 3) confinement consisted of either an outer hoop and crossties or overlapping hoops; 4) the quantity of boundary transverse reinforcement was at least 50% of that required by ACI 318-14; 5) the spacing of boundary transverse reinforcement was no larger than $8d_b$; and 6) premature anchorage failure was not reported. Table 1 contains details for 20 walls that were selected for inclusion in the database, including the cross-sectional shape of the walls, wall thickness, M/Vl_w, applied axial load, the quantity and spacing of transverse reinforcement, and the reported drift capacity.

Specimens WP1 to WP7 were so-called "wall panel" specimens that did not represent full-height cantilever walls. For these seven walls, and for three of the eight experimental programs included in the database that employed a unique loading scheme (Paulay and Goodsir 1985; Lowes et al. 2012; Brueggen et al. 2017), lateral drift capacities were approximated at the effective height (h_{eff}) of the wall to enable a direct comparison of wall panel and cantilever wall experimental results. The effective height is defined herein as the ratio of the base overturning moment-to-shear ($h_{eff} = M_b/V_b$), which is consistent with wall height (h_w) for a cantilever wall test. Drift capacities at h_{eff} (δ_u/h_{eff}) were determined by approximating elastic flexural and shear deformations above the panel test region using effective cracked and uncracked flexural and shear stiffness values recommended in ASCE 41 (ASCE/SEI 2013). For WP1 to WP7, drift predictions (δ_u/h_{eff}) made using ASCE 41 effective stiffness

Table 1–Slender wall experimental database

Author (year)	No. of tests/No. included	Cross section shape	b, in. (mm)	M/Vl_w	$P_u/A_{cv}f'_{c,test}$*	A_{sh}/A_{ACI}*	s/d_b	δ_u/h, %
(1)	(2)	(3)	(4)	(5)	(6)	(7)	(8)	(9)
Shiu et al. (1981)	2/1	Rectangular	4.0 (102)	2.9	0	0.98	2.7	2.8
Paulay and Goodsir (1985)	4/4	Rectangular (3) T-shape (1)	3.9 (100)	2.6 to 3.3	0.15 to 0.27	0.78 to 1.04	3.3 to 6.0	2.1 to 3.3
Thomsen and Wallace (1995)	4/4	Rectangular (2) T-shape (2)	4.0 (102)	3.0	0.06 to 0.09	0.46 to 0.85	3.3 to 8.0	1.3 to 2.5
Brueggen et al. (2017)	2/2	T-shape	6.0 (152)	3.5	0.04 to 0.06	0.89 to 1.28	3.2	2.1 to 2.3†
Aaleti et al. (2013)	3/2	Rectangular	6.0 (152)	2.7	0	0.83 to 0.87	4.0	2.0
Tran and Wallace (2012)	5/2	Rectangular	4.0 (102)	2.0	0.07	0.84 to 1.08	2.7 to 4.0	3.0 to 3.1
Lowes et al. (2012)	4/4	Rectangular	6.0 (152)	2.0 to 2.8	0.10 to 0.13	1.30 to 1.76	4.0	1.2 to 1.9†
Matsubara et al. (2013)	3/1	Rectangular	4.7 (120)	3.0	0.07	1.09	3.5	2.5†

*Determined using test-day material properties.

†Specimen did not represent full height cantilever wall.

Note: $P_u/A_{cv}f'_{c,test}$ is axial stress ratio; A_{sh}/A_{ACI} is ratio of the area of confining reinforcement provided (A_{sh}) to that required by ACI 318-14 (A_{ACI}); s/d_b is ratio of boundary transverse reinforcement spacing (s) to longitudinal bar diameter (d_b); and δ_u/h is reported drift capacity.

recommendations were similar to those made using experimentally measured effective stiffness values. To be consistent with the DBD formulation of Eq. (2a) to (2c), which only accounts for flexural behavior, the flexural contribution to δ_u/h_{eff} was determined for each of the walls included in the study by subtracting shear deformations. In addition, plastic flexural drift capacity and plastic rotation capacity were determined for each of the database walls. Figure 6 reports the total drift capacity (δ_u/h_{eff}), flexural drift capacity (δ_{fu}/h_{eff}), and plastic flexural drift capacity ($\delta_{f,pu}/h_{eff}$) for each of the database walls and the seven specimens tested by Segura and Wallace (2018). Total drift capacities for the walls included in the study ranged between 1.2% and 4.0%. The percent contribution of δ_{fu} and $\delta_{f,pu}$ to total drift capacity is indicated in the figure for each wall. On average, plastic flexural drift comprised 70% of the total response, and elastic flexural drift accounted for 17% of the total response. The remainder is attributed to shear, which tends to be relatively small (approximately 13% on average for the walls in the database) for slender walls. Further details about the methods used to approximate wall panel lateral drift capacities and to determine flexural deformations for each of the walls can be found in Segura (2017).

For 19 of the walls included in the study, confinement consisted of a single outer hoop with or without crossties, which is a detail allowed by ACI 318-14 for transverse reinforcement at wall boundaries. For these specimens, the plastic drift capacities reported in Fig. 6 were compared to predicted drift capacities determined according to Eq. (2b) and (2c) using the range of extreme fiber compression strain limits identified for WP1 to WP7 (Fig. 5: ε_{cu} = 0.008 to 0.012). The compression strain limits in Fig. 5 correspond to a gauge length of $l_w/2$; therefore, a plastic hinge length of $l_p = l_w/2$ was assumed, making it possible to approximate plastic rotation capacity as a function of c/l_w (Eq. (2c)), plotted in Fig. 7(a) for ε_{cu} = 0.008 and ε_{cu} = 0.012. The results plotted in Fig. 7(a) demonstrate that rotation capacity generally decreases as c/l_w increases. As shown in Fig. 7(a),

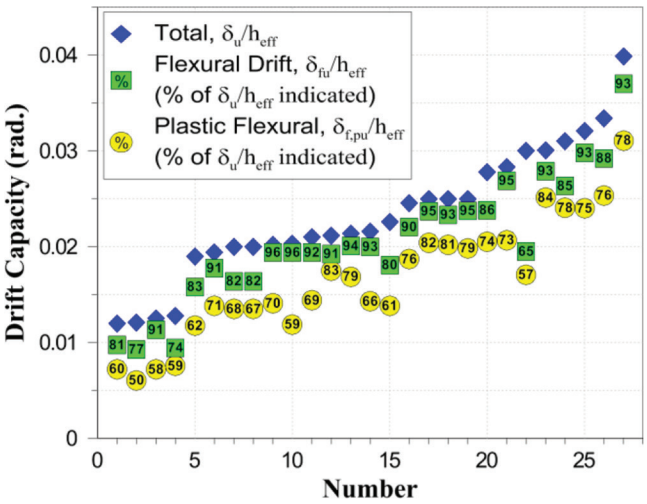

Fig. 6—Total drift capacity, flexural drift capacity, and plastic flexural drift capacity at effective height.

rotation capacity is significantly overestimated for approximately one-third of the walls in the study, even though the range of predicted plastic rotation capacity, using ε_{cu} = 0.008 and 0.012, is relatively large for a given c/l_w. In Fig. 7(b), the ratio of measured-to-predicted plastic drift capacity ($\delta_{f,pu}/\delta_{f,p\_predicted}$) is presented for each of the walls. The predicted drift capacities in Fig. 7(b) were determined according to Eq. (2b), which is the more complex form of Eq. (2c) (that is, Fig. 7(a)). The ratio of wall length-to-thickness (l_w/b) is indicated on the horizontal axis. It is observed that the best plastic drift predictions ($\delta_{f,pu}/\delta_{f,p\_predicted} \approx 1$) are made for the walls with l_w/b = 15, which is understandable because l_w/b was 15 for five of the seven tests used to define the strain limits used for the prediction (Fig. 2). However, drift capacity is overestimated ($\delta_{f,pu}/\delta_{f,p\_predicted} < 1$) for the walls with the largest length-to-thickness ratio ($l_w/b \geq 15$) and underestimated for walls such that $l_w/b \leq 10$. It is important to point out that a plastic hinge length related to wall length ($l_p = l_w/2$) was assumed for all results plotted in Fig. 7(a) and

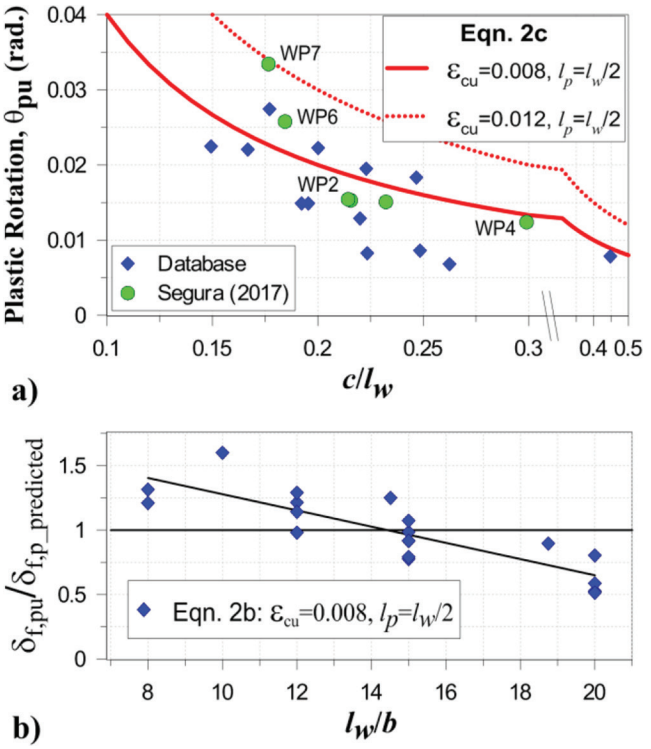

Fig. 7—(a) Plastic flexural drift capacity versus c/l_w *for walls with single outer hoop and crosstie confinement detail; and (b) ratio of measured-to-predicted plastic flexural drift capacity versus wall length-to-thickness ratio (*l_w/b*).*

7(b). Based on this assumption, two walls of the same length ($l_{w,1} = l_{w,2}$), designed for the same compression depth ($c_1 = c_2$), and with different wall thickness ($b_1 > b_2$), are predicted to have the same drift or rotation capacities (Eq. (2b) and (2c)) because c/l_w is the same for the two walls. This contradicts experimental observations reported by Segura and Wallace (2018), which indicate wall thickness influences plastic drift/rotation capacity. It is noted that Specimens WP2 (b = 6 in. [152 mm]), WP6 (b = 7.5 in. [191 mm]), and WP7 (b = 9 in. [229 mm]) exhibited a wide range of plastic rotation capacities (Fig. 7(b)), between 1.5% and 3.4%, even though c/l_w was comparable for the three walls (c/l_w = 0.18 to 0.22). On the other hand, plastic rotation capacities for Specimens WP2 (θ_{pu} = 1.5%) and WP4 (θ_{pu} = 1.2%), which were both 6 in. (152 mm) thick, were similar over a wider range of c/l_w (c/l_w = 0.22 to 0.30). Both observations indicate that using $l_p = l_w/2$ to approximate the plastic rotations in Fig. 7(a) is not suitable. Researchers have indicated that inelastic compression behavior (crushing/spalling of concrete and buckling of longitudinal reinforcement) occurs over a short height in thin wall sections, and it has been suggested that a plastic hinge length related to wall thickness ($l_p = \alpha b$, where α is a constant) may be better suited to estimate the plastic curvature capacity of thin walls (Wallace 2012; Takahashi et al. 2013; Arteta 2015). In this case, Eq. (2c) can be expressed directly in terms of wall thickness and compression depth (Eq. (4))

$$\frac{\delta_{f,p}}{h_w} \approx \frac{\alpha \varepsilon_c}{c/b} \tag{4}$$

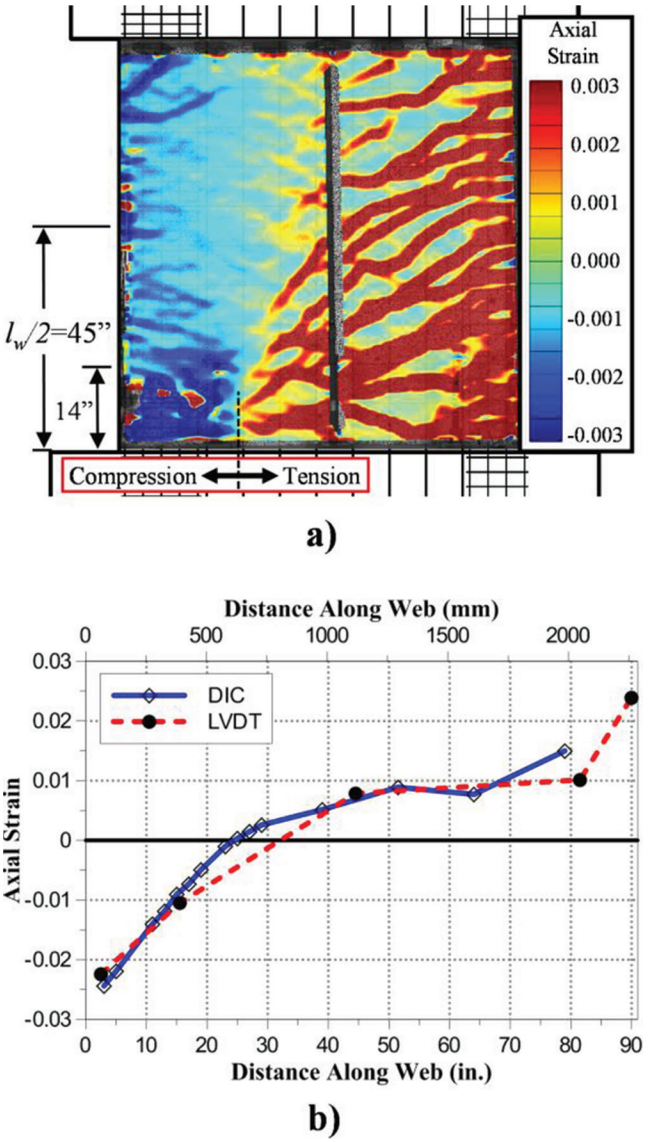

Fig. 8—Specimen WP4 axial strains prior to failure (+1.5%): (a) full axial strain field determined from digital image correlation (DIC) analysis; and (b) comparison of average axial strains measured within bottom 14 in. (356 mm) of wall using DIC and LVDT sensors (DIC analysis conducted with Optecal [Barthès 2015]).

Field and laboratory observations suggest α-values ranging between approximately 1.0 and 3.0; that is, crushing and spalling of concrete have been observed to occur over a height of one to three times the thickness of the wall. Figure 8(a) presents the full axial strain field, determined from digital image correlation analysis (Barthès 2015), for specimen WP4 at the loading step just prior to strength loss. Inelastic tension strains (approximately $\varepsilon \geq 0.002$) were well distributed up the height of the wall; however, softening occurred in the compression zone following crushing/spalling of cover concrete, and inelastic compression strains ($\varepsilon \leq -0.002$) concentrated over a short height at the base of the wall. Similar behavior was observed for all seven tests specimens (WP1 to WP7) with compression strains concentrating within the bottom 14 in. (356 mm) of the walls, corresponding to α-values between 1.6 (b = 9 in. [229 mm]) and

2.3 (b = 6 in. [152 mm]). Figure 8(b) compares the measured axial strains, within the bottom 14 in. (356 mm) of Specimen WP4, determined using the DIC analysis and LVDT sensors. Due to softening in the compression zone, the strain profile is nonlinear and the extreme fiber tension and compression strains are nearly equal in magnitude. The behavior shown in Fig. 8 agrees with a study conducted on lightly confined walls (Takahashi et al. 2013) in which drift capacity was shown to be well predicted using $\alpha = 2.5$ with a corresponding compression strain limit of $\varepsilon_{cu} = 0.007$. However, based on the extreme fiber compression strain reported in Fig. 8(b) ($\varepsilon_{cu} > 0.02$), $\varepsilon_{cu} = 0.007$ appears to be low for walls with SBE detailing.

Figure 9(a) reports the maximum compression strains measured within the bottom 14 in. (356 mm) of the wall for Specimens WP1 to WP7. Markers are included in Fig. 9 to indicate whether strength loss occurred due to compression (abrupt boundary/web crushing) or tension rupture of longitudinal reinforcement. Markers indicating tension failure may be considered lower-bound estimates of the compression strain capacity. For cases in which compression failure was observed, compression strains ranged between 0.022 and 0.036 prior to strength loss. It is noted that average compression strains measured by sensors above the 14 in. (356 mm) height did not exceed 0.002 at any time during the test. The horizontal axis of Fig. 9(a) indicates the wall thickness of the specimens for which compression strain measurements are reported. The trend in Fig. 9(a) suggests that, as wall thickness increases, compressive strain capacity increases for a constant gauge length (l_p = 14 in. [356 mm]). The strains reported in Fig. 9(a) are regularized to wall thickness in Fig. 9(b) such that the values reported in Fig. 9(b) represent the term $\alpha\varepsilon_c$ in Eq. (4). At all the boundaries where compression failures were observed, $\alpha\varepsilon_{cu}$ exceeded 0.05 prior to strength loss.

Figure 9(c) presents the maximum tension strains measured at the boundaries of all seven walls prior to strength loss. The confinement details used at each wall boundary is indicated on the vertical axis. Wall boundaries confined by continuous transverse reinforcement (Detail BE-4) remained stable when subjected to the compression strains reported in Fig. 9(a), and strength loss was attributed to tension rupture of longitudinal reinforcement, preceded by buckling of longitudinal reinforcement in all cases. Conversely, compression failures were observed at all boundaries using crossties, regardless of whether the crossties had 90°-135° hooks (Details BE-1 and BE-2) or 135°-135° (Detail BE-3). Tension strains exceeding 0.04 were measured prior to strength loss for cases in which tension failures were observed. The results indicate a tension strain limit on the order 0.04 may be warranted, which is discussed in further detail later.

As shown in Fig. 9(a), $\alpha\varepsilon_{cu}$ exceeded 0.05 at all wall boundaries that experienced compression failures. The predicted plastic rotation capacity according to Eq. (4), using $\alpha\varepsilon_{cu}l_p = 0.05b$, is plotted in Fig. 10 along with measured plastic rotations for the walls included in the study. The data in Fig. 10 demonstrate significantly less dispersion than Fig. 7(a) ($l_p = l_w/2$), and predicted rotation capacities

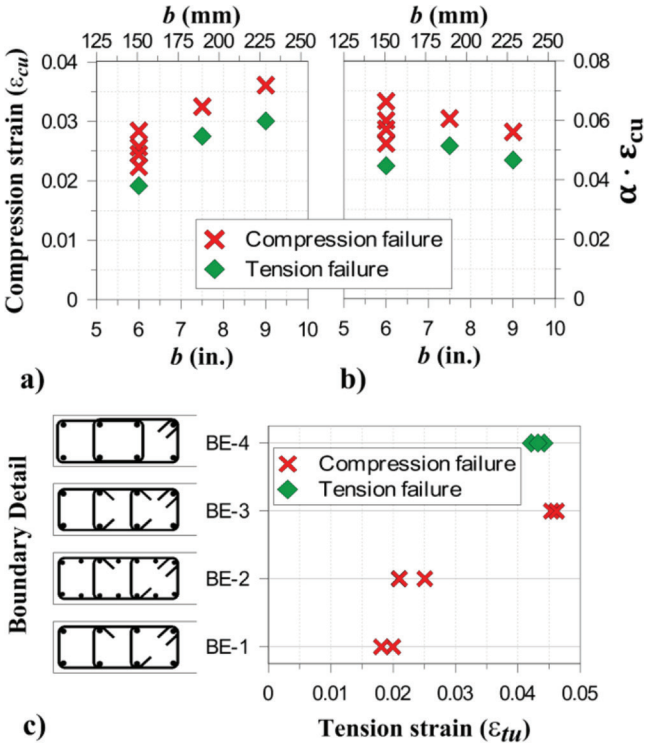

Fig. 9—(a) Maximum compression strain prior to failure measured over 14 in. (356 mm) gauge length at base of wall; b) maximum compression strain regularized to wall thickness; and c) maximum tension strain prior to failure versus confinement detail used at boundary (Detail BE-1: all longitudinal bars laterally restrained by hoop or 90°-135° crosstie; Detail BE-2: every other longitudinal bar restrained by hoop or 90°-135° crosstie; Detail BE-3: all longitudinal bars laterally restrained by hoop or 135°-135° crosstie; and Detail BE-4: all longitudinal bars laterally restrained by continuous transverse reinforcement [no crossties]).

(Eq. (4)) closely match test data using a single compression strain limit. The test data and predictive equation indicate flexural drift capacities greater than 2% may be expected for $c/b < 2.5$, and drifts less than 1% may be expected for $c/b > 5$.

While the test results in Fig. 10 appear to agree reasonably well with the prediction, rotation capacities are overestimated for a few of the walls. In Fig. 11(a), the ratio of measured-to-predicted plastic drift capacity is compared to the shear span-depth ratio (M/Vl_w), an indicator of the relative flexural and shear demands. It can be seen that $\delta_{f,p}$ is overpredicted for walls with $M/Vl_w < 3.0$ (that is, relatively high shear demand), which might suggest that the compression strain capacity of the walls with $M/Vl_w < 3.0$ is smaller than that of the relatively slender walls ($M/Vl_w \geq 3.0$). However, walls with $M/Vl_w < 3.0$ typically exhibit more notable interaction between the flexural and shear responses than relatively slender walls (Massone and Wallace 2004; Tran and Wallace 2012; Kolozvari et al. 2015). As a result, degradation of the shear-resisting mechanism may occur as wide flexural cracks open in the plastic hinge region, leading to significant nonlinear shear deformations and larger stain demands along diagonal compression struts. As shown in

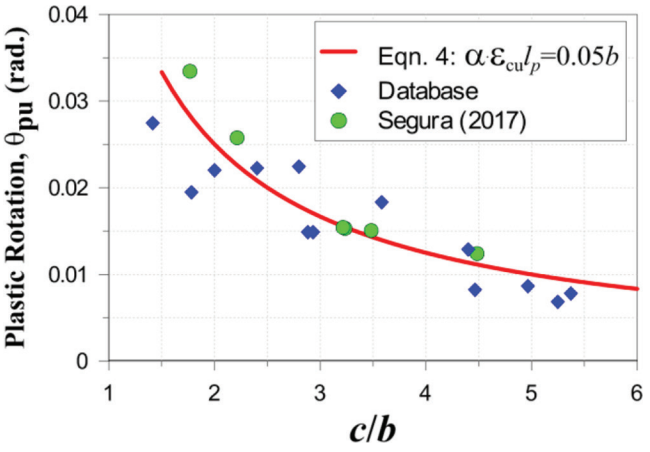

Fig. 10—Plastic rotation capacity versus c/b *for walls with single outer hoop and crosstie confinement detail.*

Fig. 11(c) and 11(d), shear deformations δ_s comprised 15 to 35% of the total response for walls with $M/Vl_w < 3.0$ and design shear stress ($v_u = V_u/A_{cv}$) greater than $3\sqrt{f'_c\,(\text{psi})}$ ($0.25\sqrt{f'_c\,[\text{MPa}]}$), while shear comprised less than 10% of the total deformation for the relatively slender walls ($M/Vl_w \geq 3.0$), which all had low shear stress demands ($v_u \leq 3\sqrt{f'_c\,[\text{psi}]}$). In Fig. 11(b), total measured plastic deformations, including shear (that is, $\delta_{pu} = \delta_{f,p} + \delta_{s,p}$), are compared to the predicted inelastic drift capacity. Inelastic shear deformations $\delta_{s,p}$ were determined by subtracting an assumed elastic contribution, estimated using the effective cracked shear stiffness values recommended in ASCE 41 ($GA_{eff} = 0.4E_cA_{cv}$). When inelastic shear is included, the predicted plastic drift capacity is reliable for all measured values of M/Vl_w and shear stress demand v_u. On average, the measured plastic drift capacity δ_{pu} is 1.19 times the predicted value, indicating that the walls with $M/Vl_w < 3.0$ likely possess similar compression strain capacity to that reported in Fig. 9(a) and 9(b), with a larger portion of the compression strain demand attributed to inelastic shear (that is, compression strut) than is observed for walls with $M/Vl_w \geq 3.0$. Further research may be necessary to quantify the impact of shear demand on the compression strain demand at wall boundaries, and to determine whether the trend shown in Fig. 11(b) ($\delta_{pu} > \delta_{f,pu\_predicted}$) applies for walls with shear stress demands close to the maximum allowed by ACI 318 ($10\sqrt{f'_c\,[\text{psi}]}$ [$0.8\sqrt{f'_c\ (\text{MPa})}$]).

Figure 10 primarily reports the drift capacities at which compression failure occurred; however, for a few of the walls, drift capacity was limited by tension rupture of longitudinal reinforcement, preceded by initial buckling of longitudinal reinforcement in all cases. At the limit state of tension rupture, Eq. (2c) can be expressed in terms of a tension strain limit ε_{tu} according to Eq. (5)

$$\frac{\delta_{f,p}}{h_w} \approx \left(\frac{\varepsilon_{tu}}{l_w - c}\right) l_p \tag{5}$$

The tension strain limits shown in Fig. 9(c) were measured over an assumed plastic hinge length of $l_p = l_w/2$. As shown in Fig. 8(a), inelastic tension strains were able to spread over

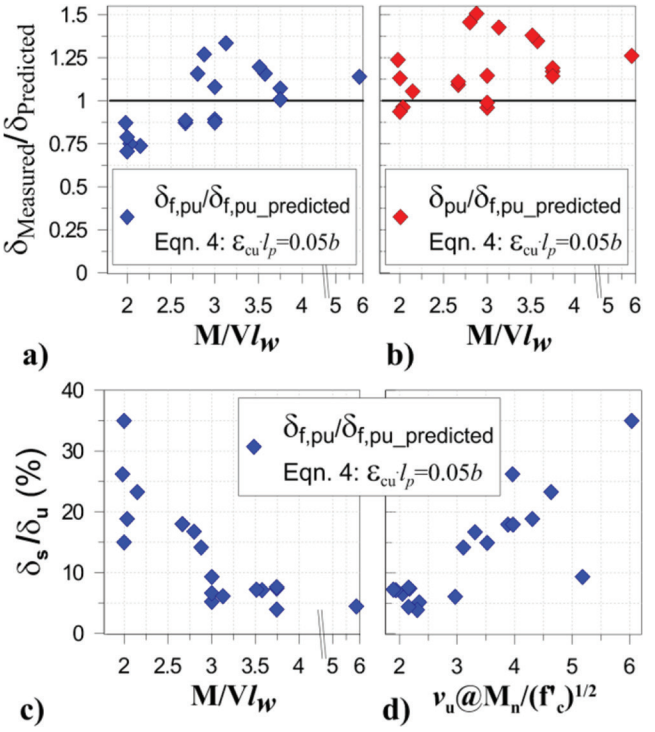

Fig. 11—(a) Ratio of measured-to-predicted plastic drift capacity versus M/Vl_w*; (b) ratio of total measured plastic drift capacity* ($\delta_{pu} = \delta_{f,pu} + \delta_{s,pu}$) *to predicted plastic drift capacity versus* M/Vl_w*; (c) percent contribution of shear deformation* (δ_s) *to total drift capacity* (δ_u) *versus* M/Vl_w*; and (d) percent contribution of shear deformation to total drift capacity versus design shear stress.*

the full height of the approximately 1.5-story panel specimens, which is approximately equal to l_w. Thus, assuming a plastic hinge length of $l_p = l_w/2$, with the tension strain limits in Fig. 9(c) ($\varepsilon_{tu} \approx 0.04$), will likely produce a lower-bound estimate of the plastic drift capacity at the limit state of tension rupture (Eq. (5)) because plastic curvature is neglected above $l_w/2$. If axial tension deformations above $l_w/2$ are considered for the specimens that reached $\varepsilon_{tu} > 0.04$, ε_{tu} is at least 0.05 when strains are regularized to $l_p = l_w/2$, which is expected to provide a more accurate estimate of the plastic drift capacity of a wall at the flexure-tension limit state.

DRIFT CAPACITY LIMIT FOR SLENDER WALLS

Equation (6) summarizes the recommended drift limit (δ_{max}/h_w) for a Special Structural Wall with SBE detailing, expressed in terms of compression depth (c), wall thickness (b), and wall length (l_w). The drift limit includes elastic deformations (δ_y/h_w) and contains terms related to the predicted drift capacities associated with the compression strain limit (Eq. (4)) and tension strain limit (Eq. (5))

$$\frac{\delta_{max}}{h_w} = \left(\frac{\delta_y}{h_w} + \frac{0.05}{c/b}\right) \leq \left(\frac{\delta_y}{h_w} + \frac{0.025}{1 - c/l_w}\right) \tag{6}$$

The elastic drift in Eq. (6) can be estimated for a given load pattern (for example, ASCE 7 Equivalent Lateral Force or Response Spectrum Analysis) using appropriate effective stiffness values (for example, ASCE 41-13). For preliminary

design, elastic drift may be estimated as $\delta_y/h_w = (11/40)\phi_y h_w$, where $\phi_y = 0.0025/l_w$ may be assumed based on the recommendations of Wallace and Moehle (1992). For simplicity, the elastic contribution may be neglected as is done in ACI 318 for determining the need for SBE detailing at wall boundaries. For the case in which elastic deformations are neglected, the drift limit of Eq. (6) is shown in Fig. 12(a) for several compression depth demands (c/l_w = 0.1 to 0.38). The drift capacity associated with the tension strain limit is shown as a horizontal line, for each c/l_w value, which places an upper limit on the allowable drift for lower wall length-to-thickness ratios (l_w/b) at which the compression strain limit will not govern the drift capacity of the wall.

The drift limits in Eq. (6) and Fig. 12(a) are intended for comparison to roof drift ratio demands (δ_u/h_w). For the walls included in the study, lateral drift ratios were measured at h_{eff}, which is less than the roof height (h_w). It is noted that plastic drift ratio is essentially constant up the height of the building ($\delta_{f,p}/h_w \approx \theta_p$ [Fig. 1(c)]); therefore, the trends in Fig. 10 and 11, which do not include elastic deformations, are valid at the roof level. However, elastic drift ratio, which comprised approximately 10 to 30% of the total drift capacity at h_{eff} for the database walls (Fig. 6), increases with height according to Eq. 1 (that is, $\delta_{f,y}/h = \gamma\phi_y h$). Based on the ASCE 7 Equivalent Lateral Force load distribution, h_w is approximately 1.3 to 1.4 times h_{eff} for a shear wall building between 3 and 10 stories in height, and even higher for taller buildings. In Fig. 12(b), the drift limits of Eq. (6) and Fig. 12(a) (δ_{max}) are compared to the lateral roof drift capacities (δ_u at h_w) for the database walls, which were determined by amplifying elastic drifts assuming $h_w = 1.3h_{eff}$. Because shear deformations are small, they were neglected above h_{eff}. Due to the difference in height between h_{eff} and h_w, δ_u/h_w is only 6% higher than δ_u/h_{eff}, on average, for the walls in the study. It is noted that, because of the small differences between drift ratios at h_w and h_{eff}, amplification of elastic drifts was not very sensitive to the choice of h_w/h_{eff}. As shown in Fig. 12(b), measured drift capacities at h_w are generally greater than or equal to 1.25 times the drift limit of Fig. 12(a) (that is, elastic deformations neglected), except for a few walls for which $\delta_u/h_{eff} > 3\%$ (δ_u/h_{eff} indicated on horizontal axis), which is acceptable given the large observed deformation capacity. When elastic deformations are included (Eq. (b)), δ_u/δ_{max} is close to 1.0 for most of the walls.

For new building design (ASCE 7; ACI 318), the design drift ratio (δ_u/h_w) is based on Design Earthquake (DE) demands that are assumed as two-thirds of MCE demands. Equation (6) is a limit state formulation, intended for collapse prevention, which makes it more suitable for comparison to MCE demands. In this case, the design drift ratio (δ_u/h_w) and drift limit (δ_{max}/h_w) should be compared in accordance with Eq. (7)

$$\frac{1.5\delta_u}{h_w} \le \frac{\delta_{max}}{h_w} \tag{7}$$

Based on the limited results presented in Fig. 12(b)—that is, δ_u/δ_{max} generally greater than or equal to 1.0—Eq. (7) is expected to provide a low probability of collapse for a shear wall building subjected to MCE demands, consistent with the building code intent. A detailed reliability study, using a larger database of experimental tests, may help to further explore the level of reliability associated with the use of Eq. (7) for DE and MCE demands.

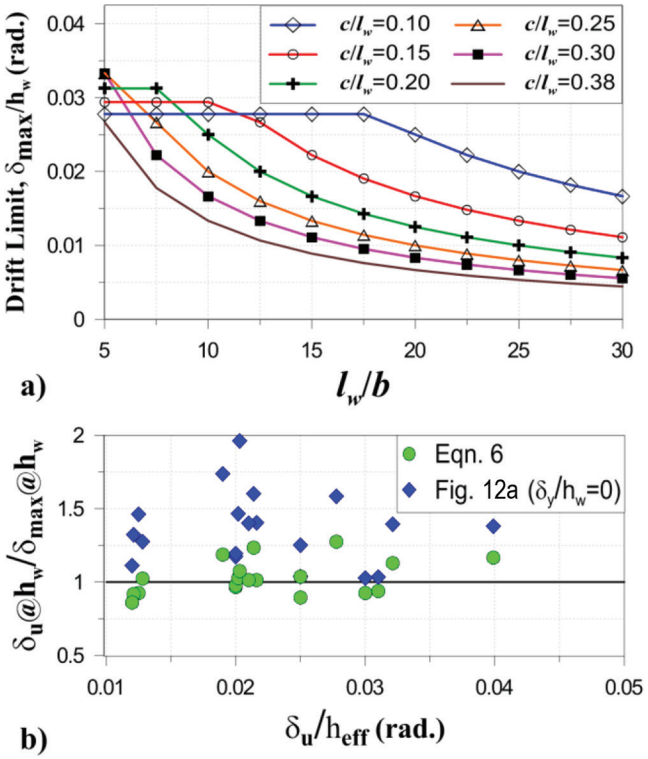

Fig. 12—(a) Recommended drift capacity limit for Special Structural Walls with SBEs; and (b) comparison of measured drift capacities and drift limit.

In Fig. 13, plastic rotation capacities for walls with overlapping hoop configurations, which are not included in Fig. 10, are compared to those with hoop and crosstie configurations. In general, the walls with overlapping hoops demonstrate larger plastic rotation capacities for a given c/b. Linear trend lines suggest walls with overlapping hoops possess approximately 1% more drift capacity, on average, for a given value of c/b. According to Fig. 13, it may be reasonable to allow drifts larger than those recommended in Fig. 12(a) if transverse reinforcement is provided by overlapping hoops. A detailed survey of monotonic and cyclic tests on code compliant boundary element specimens may help to quantify the compression and tension strain limits for transverse reinforcement exceeding that required by ACI 318-14. It is noted that the drift capacity for walls designed with enhanced detailing may be governed by tension rupture of longitudinal reinforcement except for walls with moderate or large compression depths (that is, $c/b \ge 4$).

SUMMARY AND CONCLUSIONS

Experimentally measured flexural drift capacities were presented for a small database of walls with well-detailed boundary zones. The measured drift capacities were compared to a drift limit formulation developed in a displacement-based design (DBD) format. The drift limit was calibrated based on axial (flexural) compression and

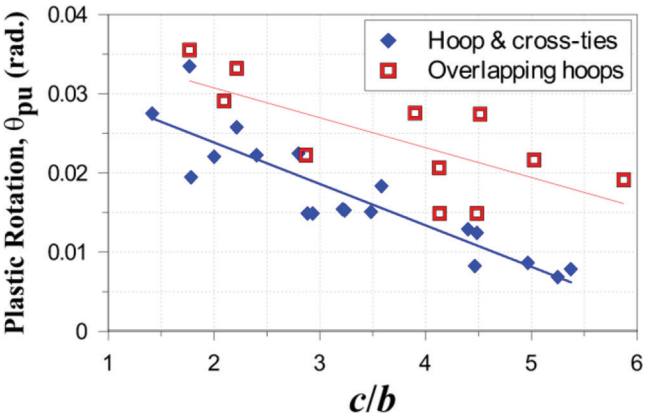

Fig. 13—Plastic rotation capacity versus c/b*: impact of boundary transverse detailing.*

tension strain limits identified in seven wall tests conducted as part of this experimental program. The following observations and conclusions are made:

1. Experimental data indicate that drift capacity increases as wall thickness (b) increases for a given compression depth (c). A lateral drift limit equation was formulated in a displacement-based design (DBD) format, based on experimentally measured compression strain and tension strain limits, and good agreement of the drift limit with experimental data was observed for relatively slender walls ($M/Vl_w \geq 3.0$). The predictive equation and test data indicate drift capacities greater than 2% may be expected for code-compliant walls designed such that the compression depth is less than 2.5 times the wall thickness ($c/b < 2.5$), while drift capacities less than 1% are expected for walls with $c/b > 5$. Additional research is suggested to quantify the impact of shear span-depth ratio (M/Vl_w) and shear stress on the compression strain demands at wall boundaries.

2. For DBD, it is common to assume a plastic hinge length of one-half the length of the wall in order to capture inelastic curvature. It was shown that drift predictions using a DBD format may be unconservative for relatively long walls (that is, $l_w/b \geq 15$), and overly conservative for shorter walls (that is, $l_w/b \leq 10$), when compression strain capacity is assumed to be constant (for example, $\varepsilon_{cu} = 0.008$) and plastic hinge length is assumed to be related to wall length. This is because drift capacity is assumed to be directly related to the ratio of compression depth to wall length (c/l_w). By this definition, two walls with the same c/l_w and different wall thicknesses are expected to possess similar drift capacity, although it has been shown that thinner walls tend to be less ductile.

3. For thick walls and/or walls designed for relatively low compression (for example, $c/b < 3$), drift capacity may be limited by tension rupture of longitudinal reinforcement. A tension strain limit of 0.05, with an associated plastic hinge length of $l_p = l_w/2$, is suggested based on a review of limited test data.

4. Based on the information presented, equivalent performance is not expected for all walls that satisfy ACI 318-14 provisions. Walls with lower c/b and/or overlapping hoop confinement are more stable in compression, making it possible to achieve larger inelastic deformations. An approach that involves comparing drift demands to drift capacities for individual walls is presented that would enable a designer to make informed decisions about the impact of building (wall) layout and wall proportioning and detailing on expected building performance. Another approach might be to suggest a minimum wall thickness and/or minimum detailing requirements to achieve a given drift demand. A detailed survey of monotonic and cyclic tests on code-compliant boundary element specimens is suggested to quantify the compression and tension strain limits of confinement details exceeding ACI 318-14 requirements.

AUTHOR BIOS

ACI member **Christopher L. Segura Jr.** *was formerly a PhD Student at the University of California, Los Angeles (UCLA), Los Angeles, CA. He is now a Research Structural Engineer at the National Institute of Standards and Technology. He received his BS and MS from the University of Colorado, Boulder, CO. He is a member of ACI Committees 133, Disaster Reconnaissance, and 369, Seismic Repair and Rehabilitation. His research interests include seismic design and laboratory testing of reinforced concrete structures.*

John W. Wallace, *FACI, is a Professor of civil engineering at UCLA. He is a member of ACI Committees 318, Structural Concrete Building Code; 318-H, Seismic Provisions; 369, Seismic Repair and Rehabilitation; and 374, Performance-Based Seismic Design of Concrete Buildings. His research interests include response and design of buildings and bridges to earthquake actions, laboratory and field testing of structural components and systems, and seismic structural health monitoring.*

ACKNOWLEDGMENTS

The work presented in this paper was supported by funds from the National Science Foundation (NSF) Grant No. CMMI-1208192. The reported experiments were conducted in a laboratory renovated with funds provided by the NSF under Grant No. 0963183. This financial support is gratefully acknowledged.

NOTATION

A_{cv}	=	gross area of concrete bounded by web thickness and length
b	=	width of compression face
c	=	distance from extreme compression fiber to neutral axis
d_b	=	nominal diameter of bar
E_c	=	modulus of elasticity of concrete
E_s	=	modulus of elasticity of reinforcing steel
f_c'	=	specified compressive strength of concrete
f_y	=	specified yield strength of reinforcement
l_w	=	length of wall in direction of shear force
s	=	center-to-center spacing of transverse reinforcement

REFERENCES

Aaleti, S.; Brueggen, B. L.; Johnson, B.; French, C. E.; and Sritharan, S., 2013, "Cyclic Response of Reinforced Concrete Walls with Different Anchorage Details: Experimental Investigations," *Journal of Structural Engineering*, ASCE, V. 139, No. 7, pp. 1181-1191. doi: 10.1061/(ASCE)ST.1943-541X.0000732

ACI Committee 318, 2014, "Building Code Requirements for Structural Concrete (ACI 318-14) and Commentary (ACI 318R-14)," American Concrete Institute, Farmington Hills, MI, 520 pp.

Arteta, C. A., 2015, "Seismic Response Assessment of Thin Boundary Element Specimens of Special Concrete Shear Walls," PhD dissertation, University of California, Berkeley, Berkeley, CA, 240 pp.

ASCE/SEI, 2010, "Minimum Design Loads for Buildings and Other Structures (ASCE/SEI 7-10)," American Society of Civil Engineers, Reston, VA.

ASCE/SEI, 2013, "Seismic Evaluation and Retrofit of Existing Buildings (ASCE/SEI 41-13)," American Society of Civil Engineers, Reston, VA.

Barthès, C. B., 2015, Optecal (Computer software: www.optecal.com).

Brueggen, B. L.; French, C. E.; and Sritharan, S., 2017, "T-Shaped RC Structural Walls Subjected to Multidirectional Loading: Test Results and Design Recommendations," *Journal of Structural Engineering*, ASCE, V. 141, No. 5, pp. 1-15 doi: 10.1061/(ASCE)ST.1943-541X.0001719

Kolozvari, K.; Orakcal, K.; and Wallace, J. W., 2015, "Modeling of Cyclic Shear-Flexure Interaction in Reinforced Concrete Structural Walls

– Part I: Theory," *Journal of Structural Engineering*, ASCE, V. 143, No. 7, pp. 1-10. doi: 10.1061/(ASCE)ST.1943-541X.0001059

Lowes, L. N.; Lehman, D. E.; Birely, A. C.; Kuchma, D. A.; Marley, K. P.; and Hart, C. R., 2012, "Earthquake Response of Slender Planar Concrete Walls with Modern Detailing," *Engineering Structures*, V. 43, pp. 31-47. doi: 10.1016/j.engstruct.2012.04.040

Massone, L. M., 2013, "Fundamental Principles of the Reinforced Concrete Design Code Changes in Chile Following the Mw 8.8 Earthquake in 2010," *Engineering Structures*, V. 56, pp. 1335-1345. doi: 10.1016/j.engstruct.2013.07.013

Massone, L. M., and Wallace, J. W., 2004, "Load-Deformation Responses of Slender Reinforced Concrete Walls," *ACI Structural Journal*, V. 101, No. 1, Jan.-Feb., pp. 103-113.

Matsubara, S.; Sanada, Y.; Tani, M.; Takahashi, S.; Ichinose, T.; and Fukuyama, H., 2013, "Structural Parameters of Confined Area Affect Flexural Deformation Capacity of Shear Walls that Fail in Bending with Concrete Crushing," *Journal of Construction Engineering* (in Japanese), V. 78, No. 691, pp. 1593-1602. doi: 10.3130/aijs.78.1593

MINVU, 2011, "Reinforced Concrete Design Code (DS No. 60)," Ministry of Housing and Urbanism, Santiago, Chile. (in Spanish)

Nagae, T.; Tahara, K.; Fukuyama, K.; Matsumori, T.; Siohara, H.; Kabeyasawa, T.; Kono, S.; Nishiyama, M.; Moehle, J.; Wallace, J.; Sause, R.; and Ghannoum, W., 2012, "Test Results of Four-Story Reinforced Concrete and Post-Tensioned Concrete Buildings: The 2010 E-Defense Shaking Table Test," *Proceedings of the 15th World Conference on Earthquake Engineering*, Lisbon, Portugal.

Oesterle, R. G.; Fiorato, A. E.; Johal, L. S.; Carpenter, J. E.; Russel, H. G.; and Corley, W. G., 1976, "Earthquake Resistant Structural Walls – Tests of Isolated Walls," *Technical Report to the National Science Foundation*, Construction Technology Laboratories, Skokie, IL, 318 pp.

Paulay, T., and Goodsir, J., 1985, "The Ductility of Structural Walls," *Bulletin of the New Zealand National Society for Earthquake Engineering*, V. 18, No. 3, pp. 250-269.

Segura, C. L., 2017, "Seismic Performance Limitations of Slender Reinforced Concrete Structural Walls," PhD dissertation, University of California, Los Angeles, Los Angeles, CA, 238 pp.

Segura, C. L., and Wallace, J. W., 2018, "Seismic Performance Limitations and Detailing of Slender Reinforced Concrete Walls," *ACI Structural Journal*, V. 115, No. 3, May, pp. 849-860. doi: 10.14359/51701918

Shiu, K. N.; Daniel, J. I.; Aristizabal-Ochoa, J. D.; Fiorato, A. E.; and Corley, W. G., 1981, "Earthquake Resistant Structural Walls – Tests of Walls With and Without Openings," *Technical Report to the National Science Foundation*, 43 pp.

Takahashi, S.; Yoshida, K.; Ichinose, T.; Sanada, Y.; Matsumoto, K.; Fukuyama, H.; and Suwada, H., 2013, "Flexural Drift Capacity of Reinforced Concrete Wall with Limited Confinement," *ACI Structural Journal*, V. 110, No. 1, Jan.-Feb., pp. 95-104.

Thomsen, J. H., and Wallace, J. W., 1995, "Displacement-Based Design of Reinforced Concrete Structural Walls: An Experimental Investigation of Walls with Rectangular and T-Shaped Cross-Sections," *Report No. CU/CEE-95-06*, Clarkson University, Potsdam, NY, 353 pp.

Tran, T. A., and Wallace, J. W., 2012, "Experimental Study of the Lateral Load Response of Moderate Aspect Ratio Reinforced Concrete Structural Walls," *Report No. UCLA-SGEL 2012/12*, University of California, Los Angeles, Los Angeles, CA, 303 pp.

Wallace, J. W., 2012, "Behavior, Design, and Modeling of Structural Walls and Coupling Beams – Lessons from Recent Laboratory Tests and Earthquakes," *International Journal of Concrete Structures and Materials*, V. 6, No. 1, pp. 3-18. doi: 10.1007/s40069-012-0001-4

Wallace, J. W., and Moehle, J. P., 1992, "Ductility and Detailing Requirements of Bearing Wall Buildings," *Journal of Structural Engineering*, ASCE, V. 118, No. 6, pp. 1625-1644. doi: 10.1061/(ASCE)0733-9445(1992)118:6(1625)

Wallace, J. W., and Orakcal, K., 2002, "ACI 318-99 Provisions for Seismic Design of Structural Walls," *ACI Structural Journal*, V. 99, No. 4, July-Aug., pp. 499-508.

Welt, T. S., 2015, "Detailing for Compression in Reinforced Concrete Wall Boundary Elements: Experiments, Simulations, and Design Recommendations," PhD dissertation, University of Illinois at Urbana-Champaign, Champaign, IL, 530 pp.